Int. J. Heat Mass Transfer. Vol. 28, No. 9, pp. 1645–1656, 1985
Printed in Great Britain

0017–9310/85 $3.00 + 0.00
Pergamon Press Ltd.

Heat transfer in tube banks under conditions of turbulent inclined flow

K. A. ANTONOPOULOS

National Technical University of Athens, Mechanical Engineering Department, Thermal Section, 42 Patission Street, Athens 106 82, Greece

(*Received* 19 *September* 1984)

Abstract—The present paper is concerned with the prediction of heat transfer in banks of tubes under conditions of turbulent fully-developed flow inclined to the axes of the tubes, including the limiting cases of purely axial and purely transverse flow. The differential equations governing flow and heat transfer are expressed in curvilinear coordinates and solved by finite-difference means. The effects of turbulence are simulated by the 'k–ε turbulence model'. Results are compared with theoretical and experimental data in the cases of purely axial and purely transverse flow. Novel information is provided about the effects of flow inclination on heat transfer.

1. INTRODUCTION

THE PRESENT paper presents the heat transfer aspects of a computational study concerning turbulent flow and heat transfer in banks of tubes (Fig. 1). The hydrodynamic aspects have been presented in previous publications [1, 2].

The importance of tube-bank flows and heat transfer is too well known to require extensive repetition here; suffice it to mention their occurrence in heat exchangers, boilers, condensers and nuclear reactors. The simplest case occurs under conditions of purely 'axial' fully-developed flow (Fig. 1) as in, for example, a nuclear reactor fuel assembly consisting of rod bundles with the coolant flowing axially through the bundles in the spaces between the rods. A more complex two-dimensional case occurs under conditions of purely 'transverse' fully-developed flow (Fig. 1) as, for example, happens in those heat exchangers where flow is directed normal to the axes of the tubes.

Although the above-mentioned limiting cases of fully-developed purely axial or transverse flow are examined in the present work, the main interest lies in circumstances where the flow is inclined to the axes of the tubes. Such cases are encountered in many types of industrial equipment including heat exchangers with baffles or other obstructions. A further example in this class is the 'blockage' problem in liquid-metal-cooled fast-breeder nuclear reactors, which refers to the formation of a local coolant blockage within one or more subchannels of the rod bundle.

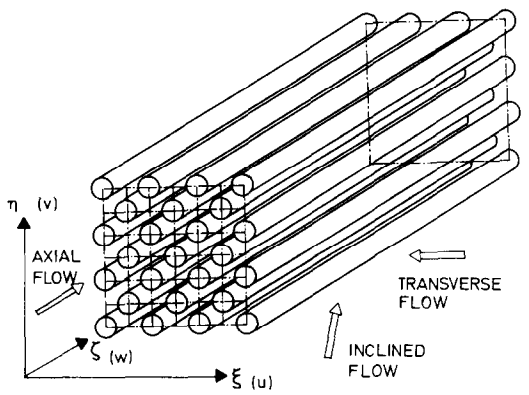

FIG. 1. Illustration of tube-bank flow.

Previous theoretical analyses of heat transfer in banks of tubes have been confined, almost without exception, to the limiting cases of purely axial and purely transverse flow mentioned above. The studies of Sparrow *et al.* [3] (laminar), Dwyer and Berry [4], Pfann [5] and Deissler and Taylor [6] (turbulent) are typical of the first case and those of Le Feuvre [7] and Massey [8] (laminar and turbulent) of the second. A full survey of theoretical and experimental studies on heat transfer in tube banks may be found in [1].

In the present study, an attempt is made to give an insight into the hitherto almost unexplored case of heat transfer under conditions of turbulent fully-developed flow inclined to the tube axes. The method of approach is numerical, i.e. the continuity, momentum and energy differential equations are solved by finite-difference means in conjunction with the 'k–ε turbulence model' [9] and associated wall functions [9] for the simulation of turbulence effects. The method, in its general form, is capable of predicting turbulent three-dimensional flow and heat transfer for arbitrary circumstances. The results presented here, however, correspond to heat transfer under conditions of fully-developed inclined flow including the limiting cases of 0° and 90° inclination (i.e. fully-developed purely axial and purely transverse flow, respectively). The latter cases serve mainly for making comparisons of the present predictions with existing experimental data in order to assess the accuracy of the method since no such data are available for comparing the heat transfer predictions in the case of flow inclined to the tube axes.

NOMENCLATURE

A_c cross-sectional area of a subchannel
a coefficient in finite-difference equations
c_p specific heat at constant pressure
D tube diameter
D_h hydraulic diameter, $4(A_c/P_w)$
E constant, 9.793
K thermal conductivity
k kinetic energy of turbulence
l_ξ, l_η metric coefficients associated with the coordinates ξ and η, respectively
$\dot{m}_a, \dot{m}_c$ mass flow rate in the axial and transverse directions respectively
$\overline{Nu}$ average Nusselt number,

$$\frac{1}{\pi(D/2)}\int_{0^\circ}^{180^\circ}\frac{\dot{q}''_w D}{K(T_w-T_b)}\frac{D}{2}\,d\phi,$$

where $T_b = T_{bI}$ for $0^\circ \leqslant \phi \leqslant 90^\circ$ and $T_b = T_{bO}$ for $90^\circ < \phi \leqslant 180^\circ$
$\overline{Nu}^h$ average Nusselt number based on the hydraulic diameter D_h,

$$\frac{1}{\pi(D/2)}\int_{0^\circ}^{180^\circ}\frac{\dot{q}''_w D_h}{K(T_w-T_b)}\frac{D}{2}\,d\phi,$$

where $T_b = T_{ba}$ for purely axial flow and $T_b = T_{bI}$ for inclined flow
P distance between axes of parallel tubes (pitch)
Pr Prandtl number, $\mu c_p/K$
Pr_t turbulent Prandtl number, $=1$
P_w wetted perimeter
p local pressure
$\dot{Q}$ total heat input to the solution domain per unit of time
$\dot{q}''_w$ local wall heat flux
Re^h Reynolds number of an inclined flow based on the hydraulic diameter, $\rho\bar{U}D_h/\mu$
Re_c transverse Reynolds number, $\rho\bar{u}D/\mu$
Re_a^h axial Reynolds number based on the hydraulic diameter, $\rho\bar{w}D_h/\mu$
St local Stanton number,

$$\frac{\dot{q}''_w}{\rho\bar{u}c_p(T_w-T_{bI})}$$

S_T, S_L transverse and longitudinal pitch to diameter ratios, respectively
S_Φ source term in the transport equations
T local fluid temperature
T_b bulk fluid temperature taken as T_{ba}, T_{bI} or T_{bO} depending on the case
T_{ba} bulk fluid temperature in the cross-sectional plane,

$$\frac{1}{A_c\bar{w}}\int_{A_c} wT\,dA_c$$

T_{bI} bulk fluid temperature at the inlet of the cross-section,

$$\int_{in}\rho uc_pT\,d\eta\Big/\int_{in}\rho uc_p\,d\eta$$

T_{bO} bulk fluid temperature at the outlet of the cross-section,

$$\int_{out}\rho uc_pT\,d\eta\Big/\int_{out}\rho uc_p\,d\eta$$

T_w local wall temperature
$\bar{U}$ mean velocity in the direction of an inclined flow
u, v, w velocity components in the ξ, η, ζ directions, respectively
$\bar{u}$ mean transverse velocity through the minimum cross-section
$\bar{w}$ mean axial velocity.

Greek symbols
$\Gamma_{\Phi,eff}$ effective exchange coefficient for property Φ
ε volumetric rate of dissipation of kinetic energy of turbulence
ζ rectilinear coordinate in the axial direction
ξ, η curvilinear–orthogonal coordinates on the cross-sectional plane
Θ angle of inclination of the bulk velocity to the tube axes, $\Theta = \arctan(\bar{u}/\bar{w})$
κ constant, 0.4187
μ molecular viscosity
μ_{eff} effective viscosity
ρ fluid density
τ_w local wall shear stress
Φ general dependent variable which may stand for u, v, w, k, ε, T
ϕ angular position of a point on tube surface measured from the rear of the tube.

2. ANALYSIS

2.1. *Coordinate system and differential equations*

One of the novel points in the present method is that the governing differential conservation equations of an arbitrary three-dimensional flow and heat transfer are expressed and solved in terms of general curvilinear-orthogonal coordinates ξ, η in the passage cross-section and a rectilinear coordinate ζ in the axial direction, as shown in Fig. 3. This formulation allows any selected solution domain, as for example those shown in the cross-sectional view of Fig. 2 or in the enlarged

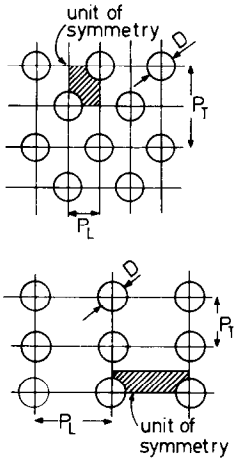

FIG. 2. Unit of symmetry (solution domain) of staggered and in-line tube banks in cross-sectional view.

isometric view of Fig. 3, to be mapped by grids which conform to its shape. A typical curvilinear–orthogonal grid, which is computer-generated by a numerical procedure described in [1], is shown in Fig. 4. This grid arrangement possesses the advantages that grid lines are aligned with the flow thus reducing numerical diffusion and that all boundaries of the solution domain are grid lines, so the imposition of the boundary conditions is straightforward and accurate.

The transport equations governing steady three-dimensional flow and heat transfer in terms of the coordinates ξ, η, ζ may be written in the following common form:

$$\frac{1}{l_\xi l_\eta}\frac{\partial}{\partial\xi}(\rho u l_\eta \Phi) + \frac{1}{l_\xi l_\eta}\frac{\partial}{\partial\eta}(\rho v l_\xi \Phi) + \frac{\partial}{\partial\zeta}(\rho w \Phi) - \frac{1}{l_\xi l_\eta}\frac{\partial}{\partial\xi}\left(\Gamma_{\Phi,\mathrm{eff}}\frac{l_\eta}{l_\xi}\frac{\partial\Phi}{\partial\xi}\right) - \frac{1}{l_\xi l_\eta}\frac{\partial}{\partial\eta}\left(\Gamma_{\Phi,\mathrm{eff}}\frac{l_\xi}{l_\eta}\frac{\partial\Phi}{\partial\eta}\right) - \frac{\partial}{\partial\zeta}\left(\Gamma_{\Phi,\mathrm{eff}}\frac{\partial\Phi}{\partial\zeta}\right) = S_\Phi \tag{1}$$

and the continuity equation may be written as:

$$\frac{1}{l_\xi l_\eta}\frac{\partial}{\partial\xi}(\rho u l_\eta) + \frac{1}{l_\xi l_\eta}(\rho v l_\xi) + \frac{\partial}{\partial\zeta}(\rho w) = 0. \tag{2}$$

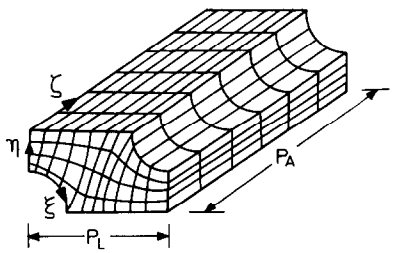

FIG. 3. Typical solution domain mapped with curvilinear–orthogonal computational mesh.

In equation (1) Φ is the dependent variable and may stand for the value of any of the following quantities: the velocity components u, v, w, in the ξ, η, ζ directions, respectively; the temperature T; the kinetic energy of turbulence k; and the volumetric rate of dissipation of kinetic energy of turbulence. The latter two quantities are associated with the 'k–ε turbulence model' employed for the simulation of turbulence effects details of which may be found in [9]. The spatially-varying metric coefficients l_ξ and l_η, which link increments of curvilinear coordinates ξ and η, respectively, with physical distance, are calculated by the grid generation procedure [1] mentioned earlier.

The term S_Φ in equation (1) stands for the source (or sink) of quantity Φ. Thus, when Φ stands for the velocity components, S_Φ contains the appropriate pressure gradient term as well as terms arising from coordinate curvature; when Φ stands for temperature, S_Φ is zero; and when Φ stands for k or ε, S_Φ contains generation and dissipation terms according to the turbulence model [9]. The full expressions of S_Φ for each case may be found in [1].

The coefficient $\Gamma_{\Phi,\mathrm{eff}}$ in equation (1) is the 'effective exchange coefficient' for property Φ. Thus, when Φ stands for the velocity components, $\Gamma_{\Phi,\mathrm{eff}}$ is the 'effective viscosity' μ_{eff}, which is given by:

$$\mu_{\mathrm{eff}} = \mu + 0.09\rho k^2/\varepsilon \tag{3}$$

where μ is the molecular viscosity. When Φ stands for k or ε, $\Gamma_{\Phi,\mathrm{eff}}$ is the 'effective diffusivity' [9] for k or ε; and when Φ stands for the temperature T, where the interest of the present paper is focused, $\Gamma_{\Phi,\mathrm{eff}}$ is given by:

$$\Gamma_{\Phi,\mathrm{eff}} = \Gamma_{T,\mathrm{eff}} = \frac{0.09\rho k^2/\varepsilon}{Pr_t} + \frac{\mu}{Pr} \tag{4}$$

where Pr is the Prandtl number and Pr_t is a 'turbulent Prandtl number', which according to [9, 10] may vary from 0.5 to 1.2 depending on the flow conditions. In the present work Pr_t has been chosen to be 1, because this is the appropriate value when the dominant resistance to heat transfer occurs near a wall.

2.2. *Boundary conditions*

The boundaries of the solution domain (Fig. 3) include symmetry planes, solid walls and inlet and outlet planes.

On a symmetry plane the velocity normal to the symmetry plane is zero as are the normal gradient of temperature and of all other variables.

The imposition of boundary conditions on the tube walls is performed by use of 'wall functions', details of which may be found in [1, 9]. Thus, for the temperature, where the interest of the present paper is focused, the treatment of boundary conditions on tube walls is as follows: in the case of prescribed wall heat flux boundary condition, the prescribed heat flux $\dot{q}''_w$ is directly used to the solution procedure. In the case of prescribed surface temperature T_w, however, it is desired for reasons of accuracy and economy [1] of the

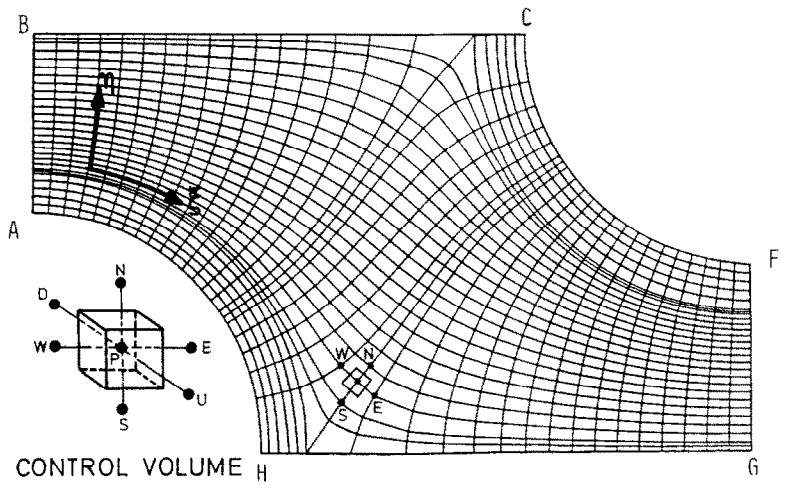

FIG. 4. Typical computational mesh (cross-sectional view) with indication of control volume.

solution to calculate the heat flux $\dot{q}''_w$ at the nearest to the wall grid points P. This calculation is performed by using the relation

$$\dot{q}''_w = K\frac{T_w - T_P}{y_P} \tag{5}$$

if point P lies in the viscous sublayer or by relation [11]:

$$\dot{q}''_w = \frac{c_p(T_w - T_P)\sqrt{\tau_w/\rho}}{Pr_t\left[\frac{1}{\kappa}\ln\left(E\frac{\rho y_P}{\mu}\sqrt{\tau_w/\rho}\right)+F\right]} \tag{6}$$

if point P lies within the turbulent region. In the above equations (5) and (6) K and c_p are the thermal conductivity and specific heat, respectively; T_P is temperature at point P and y_P is the distance of this point from the wall; τ_w is the wall shear stress; κ and E are constants taken here as 0.4187 and 9.793 respectively; and F is a function of Prandtl number, given by

$$F = 9.24\left[\left(\frac{Pr}{Pr_t}\right)^{3/4} - 1\right] \times\left[1+0.28\exp\left(-0.007\frac{Pr}{Pr_t}\right)\right]. \tag{7}$$

The above function has been derived by [12] from experimental data for equilibrium flow over smooth surfaces.

The boundary conditions at inlet and outlet planes depend on the heat transfer case which is desired to be simulated. These boundary conditions and the manner of imposing them, which is one of the novelties of the present study, are discussed in Section 3, where various heat transfer cases are examined.

2.3. *Solution procedure*

The solution procedure is based on the finite-difference formulation of [13], which is suitably modified so as to incorporate the curvilinear–orthogonal coordinates. Accordingly a very brief outline of the solution procedure is given below, for the sake of completeness. Further details are available from [1].

The solution domain is subdivided into contiguous six-sided control volumes formed by coordinate planes, as shown in Fig. 4 (view in the ξ–η plane) or Fig. 3 (enlarged isometric view). The finite-difference equations for each variable are derived by approximate integration of the differential equations (1) over each control volume with the aid of assumptions about the distribution of the variables between 'nodes' centred in each control volume, so that the conservation properties of the parent equations are preserved. The arrangement of the variables is such that the velocities lie mid-way between the pressures which drive them. The assumed distributions give rise to a 'hybrid' differencing scheme of central/upwind differencing depending on the ratio of convective/diffusive flux coefficients, as described by [13]. The resulting finite-difference equations are of the form:

$$a_P\Phi_P = \sum_n a_n\Phi_n + S_{\Phi,P}$$
$$n = \mathrm{E, W, N, S, D, U} \tag{8}$$

where the as express the combined effects of convection and diffusion, $S_{\Phi,P}$ is the integrated source term and the summation is over the six neighbours (Fig. 4). The continuity equation (2) is approximated by central differences and it is used in conjunction with the momentum finite-difference equations to derive a set of equations of the general form of (8) for a field of pressure perturbations which tend to drive the velocities towards satisfying continuity, in the manner described in [13].

The sets of algebraic equations (8) for each variable that result from the above method are solved

sequentially and repeatedly. The velocities in each cycle of calculation are obtained from the momentum equations with the prevailing pressure field inserted. They are then adjusted along with the pressure field to accord with the solution of the pressure perturbation (i.e. continuity) equation. The rest of the variables are then solved for. The solution of the set of simultaneous algebraic difference equations is effected separately for each variable by a form of ADI method in conjunction with block pressure and velocity adjustments. The solution is considered converged when the residual in each of the equation diminishes below a prescribed level.

3. HEAT TRANSFER CASES EXAMINED

3.1. *Preliminary remarks*

The differential equations (1) and (2), which describe the general case of three-dimensional flow and heat transfer, are modified in the present section so as to simulate the cases of heat transfer under conditions of (a) purely axial fully-developed flow (i.e. inclination angle $\Theta = \arctan(\bar{u}/\bar{w}) = 0°$; (b) purely transverse fully-developed flow (i.e. $\Theta = 90°$) and (c) fully-developed uniformly inclined flow (i.e. $0° < \Theta < 90°$). The simplifications performed result in a considerable reduction in computer storage and time compared to that for the general case. Extracts are shown from a wide range of heat transfer predictions for the three cases mentioned above. The corresponding results concerning hydrodynamics have been presented in previous publications [1, 2].

The fineness of the grids employed for the numerical solution of the differential equations in each case have been defined by performing grid dependence tests, details of which may be found in [1].

With reference to the turbulence model employed, it ought to be mentioned that it imposes various limitations, the most important of which are:

(a) It is assumed that the flow within the tube bank is wholly turbulent and therefore transition effects cannot be simulated. The present predictions are therefore expected to be more reliable for the higher Reynolds numbers. This limitation is, however, less restricting in an inclined flow than in a purely transverse one because, for a given transverse Reynolds number, higher turbulence is expected in the former case than in the latter due to extra turbulence generation associated with the axial velocity gradients in the ξ and η directions.

(b) Turbulence-driven secondary motions, which arise in purely axial flow cannot be simulated. The heat transfer predictions in this case are, therefore, expected to be less accurate in respect of local quantities (e.g. local heat transfer coefficients) than in respect of overall heat transfer performance where the effects of secondary motions are to some extent averaged out. In the case of inclined flow, however, the inability of the turbulence model employed to simulate the turbulence-driven secondary motion, is of little importance because these are swamped by the transverse component of the inclined flow.

3.2. *Heat transfer under conditions of purely axial fully-developed flow*

3.2.1. *Equations and boundary conditions.* In the limiting case of purely axial fully-developed flow (i.e. inclination angle $\Theta = 0°$) equations (1) and (2) are simplified as follows: (a) transverse velocities u and v are set to zero ($u = v = 0$); and (b) the condition of full development of flow and heat transfer implies that all derivatives with respect to the axial coordinate ζ vanish, with the exception of terms $\partial p/\partial\zeta$ and $\partial(\rho wT)/\partial\zeta$, which are non-zero. The problem is therefore described by the following equations:

Transport equations for $\Phi = w, k, \varepsilon$

$$\frac{1}{l_\xi l_\eta}\frac{\partial}{\partial\xi}\left(\Gamma_{\Phi,\mathrm{eff}}\frac{l_\eta}{l_\xi}\frac{\partial\Phi}{\partial\xi}\right)+\frac{1}{l_\xi l_\eta}\times\frac{\partial}{\partial\eta}\left(\Gamma_{\Phi,\mathrm{eff}}\frac{l_\xi}{l_\eta}\frac{\partial\Phi}{\partial\eta}\right)=-S_\Phi. \quad (9)$$

Energy equation

$$\frac{\partial}{\partial\zeta}(\rho wT)-\frac{1}{l_\xi l_\eta}\frac{\partial}{\partial\xi}\left(\Gamma_{T,\mathrm{eff}}\frac{l_\eta}{l_\xi}\frac{\partial T}{\partial\xi}\right)-\frac{1}{l_\xi l_\eta}\frac{\partial}{\partial\eta}\left(\Gamma_{T,\mathrm{eff}}\frac{l_\xi}{l_\eta}\frac{\partial T}{\partial\eta}\right)=0. \quad (10)$$

The solution can therefore be confined to a single cross-sectional plane ξ–η with the terms $\partial p/\partial\zeta$ and $\partial(\rho wT)/\partial\zeta$, which contain the axial coordinate ζ, treated as follows: the axial pressure gradient term $\partial p/\partial\zeta$ (contained in the source term of w-momentum equation (9)) is prescribed as an input or it is adjusted during the solution procedure so that the desired mass flow rate may be obtained. Under the boundary condition of uniform wall heat flux $\dot{q}''_w$, the axial temperature gradient term $\partial(\rho wT)/\partial\zeta$ is explicitly known [14], i.e.

$$\frac{\partial}{\partial\zeta}(\rho wT)=\rho w\left(\frac{\dot{q}''_w P_w}{\dot{m}_a c_p}\right) \quad (11)$$

where $\dot{m}_a$ is the axial mass flow rate and P_w the wetted perimeter. The above value of $\partial(\rho wT)/\partial\zeta$ is inserted as a source term during the solution of the energy equation (10).

The boundary condition of constant wall heat flux is used on the solid boundaries (i.e. tube walls AH, and CF, Fig. 4) of the solution domain while on all other boundaries (i.e. AB, BC, FG and GH, Fig. 4), which are planes of symmetry, the normal gradients of temperature and velocity is set to zero.

3.2.2. *Results.* The predicted average Nusselt number $\overline{Nu}^h/Nu_{cir}$ (based on the hydraulic diameter and normalized by the corresponding values for the circular

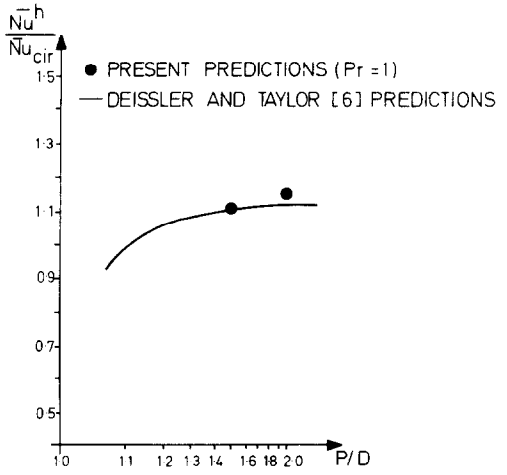

FIG. 5. Predicted average Nusselt number $\overline{Nu}^h/\overline{Nu}_{cir}$ for fully-developed axial flow through equilateral triangular arrangements at $Re_a^h = 10^5$.

duct taken from [14]) as a function of the pitch-to-diameter ratio P/D for the equilateral triangular arrangement is shown in Fig. 5 together with Deissler and Taylor [6] analytically-calculated values. Both calculations have been performed at Reynolds number $Re_a^h = 10^5$ (based on the hydraulic diameter). The agreement observed between the two calculations is very good, the maximum disagreement being less than 2%.

The variation of $\overline{Nu}^h$ with Re_a^h at Prandtl number $Pr = 1$ is shown in Fig. 6, where the present predictions for equilateral triangular arrangements of $P/D = 1.5$ and 2 are given together with the circular duct solution taken from [14]. It can be seen in this figure that for all Reynolds numbers $\overline{Nu}^h$ slightly increases with P/D by an amount which is practically independent of Reynolds number. The increase of $\overline{Nu}^h$ with P/D

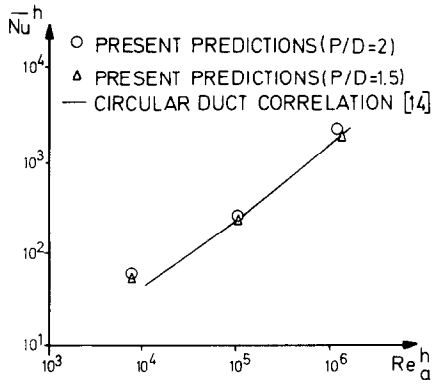

FIG. 6. Predicted average Nusselt number $\overline{Nu}^h$ for fully-developed axial flow through equilateral triangular arrangements of $P/D = 1.5$ and 2 compared with the circular duct correlation ($Pr = 1$).

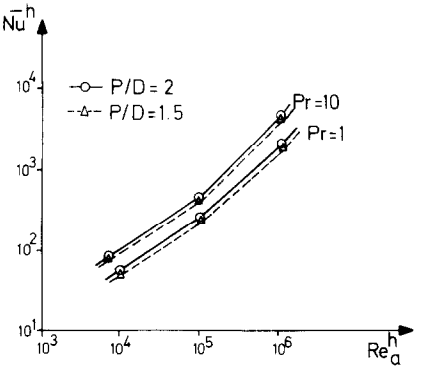

FIG. 7. Predicted average Nusselt number $\overline{Nu}^h$ for fully-developed axial flow through equilateral triangular arrangements of $P/D = 1.5$ and 2 for $Pr = 1$ and 10.

(observed in both Figs. 5 and 6 is due to the use of the hydraulic diameter for the calculation of the former. If the tube diameter is used instead, as the characteristic length, the Nusselt number decreases with increasing P/D due to decreasing velocity gradients near the tube wall.

The predicted effect of variations in Prandtl number is shown in Fig. 7, where the predicted $\overline{Nu}^h$ is given as a function of Re_a^h for $Pr = 1$ and 10, corresponding to equilateral triangular arrangements of $P/D = 1.5$ and 2. The effect of Pr is eliminated by replotting as $\overline{Nu}^h Pr^{-0.3}$ vs Re_a^h, as shown in Figs. 8 (a) and (b).

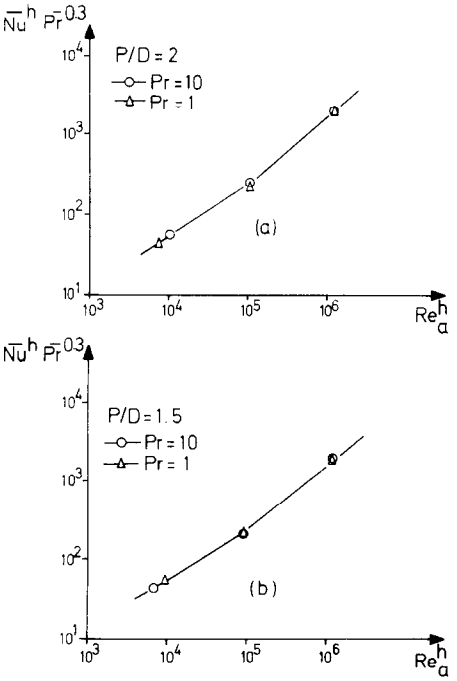

FIG. 8. Heat transfer correlation ($\overline{Nu}^h Pr^{-0.3}$ vs Re_a^h) for fully-developed axial flow through equilateral triangular arrangements of (a) $P/D = 2$ and (b) $P/D = 1.5$.

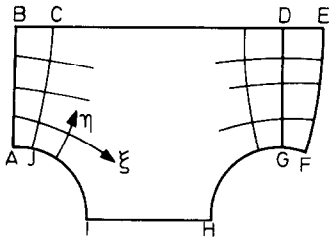

FIG. 9. Solution domain with extra row of cells at the outlet, employed for the solution of fully-developed transverse or inclined flow and heat transfer.

3.3. *Heat transfer under conditions of purely transverse fully-developed flow*

3.3.1. *Equations and boundary conditions.* In the limiting case of purely transverse fully-developed flow (i.e. inclination angle $\Theta = 90°$), the terms in the governing equations (1) and (2) relating to the axial coordinate ζ vanish and the axial velocity component w is set to zero ($w = 0$). The governing equations take, therefore, the following form:

Transport equations for $\Phi = u, v, k, \varepsilon$

$$\frac{1}{l_\xi l_\eta}\frac{\partial}{\partial \xi}(\rho l_\eta u\Phi) + \frac{1}{l_\xi l_\eta}\frac{\partial}{\partial \eta}(\rho l_\xi v\Phi) - \frac{1}{l_\xi l_\eta}\frac{\partial}{\partial \xi}\left(\Gamma_{\Phi,\mathrm{eff}}\frac{l_\eta}{l_\xi}\frac{\partial \Phi}{\partial \xi}\right) - \frac{1}{l_\xi l_\eta}\frac{\partial}{\partial \eta}\left(\Gamma_{\Phi,\mathrm{eff}}\frac{l_\xi}{l_\eta}\frac{\partial \Phi}{\partial \eta}\right) = S_\Phi. \quad (12)$$

Energy equation

$$\frac{1}{l_\xi l_\eta}\frac{\partial}{\partial \xi}(\rho l_\eta uT) + \frac{1}{l_\xi l_\eta}\frac{\partial}{\partial \eta}(\rho l_\xi vT) - \frac{1}{l_\xi l_\eta}\frac{\partial}{\partial \xi}\left(\Gamma_{T,\mathrm{eff}}\frac{l_\eta}{l_\xi}\frac{\partial T}{\partial \xi}\right) - \frac{1}{l_\xi l_\eta}\frac{\partial}{\partial \eta}\left(\Gamma_{T,\mathrm{eff}}\frac{l_\xi}{l_\eta}\frac{\partial T}{\partial \eta}\right) = 0. \quad (13)$$

Continuity equation

$$\frac{1}{l_\xi l_\eta}\frac{\partial}{\partial \xi}(\rho u l_\eta) + \frac{1}{l_\xi l_\eta}\frac{\partial}{\partial \eta}(\rho v l_\xi) = 0. \quad (14)$$

Since no variations of flow conditions exist with axial direction ζ, the solution of the above equations is confined to a single cross-sectional plane ξ–η.

The condition of full development is used for the imposition of the boundary conditions at inlet BA and outlet DG of the solution domain (Fig. 9) as follows. The computational mesh is extended by one line EF and temperature profile (as well as the profiles of the other variables) is transferred from line DG to line BA and from CJ to EF after each iteration during the solution. In this procedure, the increase in bulk fluid temperature DT_b is calculated as:

$$DT_b = \frac{\dot{Q}}{\dot{m}_c c_p} \quad (15)$$

where $\dot{Q}$ is the total heat input to the solution domain from the tubes per unit of time and $\dot{m}_c$ is the mass flow rate. DT_b is then subtracted from the temperature profile of line DG before this profile is inserted at line BA and similarly DT_b is added to temperature profile of line CJ before it is inserted at line EF.

An alternative procedure has also been devised for imposing the repeating conditions at inlet and outlet. In this procedure, which leads to faster convergence, the normal grid arrangement is used and the cyclic conditions are incorporated implicitly into the ADI algorithm.

The boundary condition of uniform heat flux $\dot{q}''_w$ is used on the solid boundaries (i.e. tube walls AJI and HGF, Fig. 9) of the solution domain while on the upper and lower boundaries BCDE and IH, respectively (Fig. 9) which are planes of symmetry, v-velocity is zero as are the normal gradients of temperature and of all other variables.

3.3.2. *Results.* The predicted distribution of local Stanton number for an in-line arrangement of transverse and longitudinal pitch-to-diameter ratios

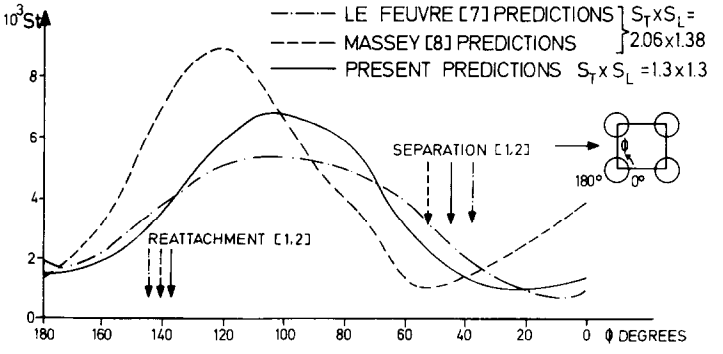

FIG. 10. Predicted distribution of local Stanton number St for fully-developed transverse flow through various in-line arrangements at $Re_c = 10^5$ and $Pr = 0.7$.

$S_T \times S_L = 1.3 \times 1.3$ at Reynolds number $Re_c = 10^5$ and Prandtl number $Pr = 0.7$, is shown in Fig. 10 together with the predictions of Le Feuvre [7] and Massey [8] for a different in-line arrangement of $S_T \times S_L = 2.06 \times 1.38$. Although the latter two sets of predictions correspond to the same flow conditions and tube spacing, remarkable disagreement is evident, which is probably due to the different level of numerical errors in the two studies.

The present predictions display the expected pattern: thus the maximum St is not obtained on the top of the tubes, as is the case with the laminar flow [1], but it is displaced towards the reattachment point where it is known [1, 2] that the turbulence level attains a maximum value. Not reproduced is the sudden change of slope (between the location of the maximum St and the separation point) which corresponds to the boundary-layer transition point and can be seen clearly in various experimental results, for example Mikhaylov [15]. This inadequacy is due to the k–ε turbulence model employed, which cannot simulate transition effects.

The predicted overall heat transfer performance for the arrangement discussed above is shown in Fig. 11 in the form of the mean Nusselt number $\overline{Nu}$ as a function of Re_c. The measurements of Stasiulevicius and Samoshka [16, 17], which are also plotted in the figure, are in very good agreement with the present predictions, especially for the higher Re_c. The transition of the laminar boundary layer to a turbulent one is manifested in the measurements as a change of slope but, of course, this cannot be reproduced in the predictions, as already mentioned.

Similar comparisons for an in-line arrangement of $S_T \times S_L = 2 \times 2$ and a fluid of $Pr = 0.7$ appear in Fig. 12. Again good agreement is observed for the higher Re_c and less good for the lower Re_c due to inapplicability of the turbulence model employed in the lower range of Reynolds number. Comparison of this figure with Fig. 11 shows that $\overline{Nu}$ is higher for the widely-spaced bank than for the closely-spaced one. This behaviour, which contradicts the corresponding behaviour in the laminar case [1], is presumably due to the influence of turbulence on the heat transfer.

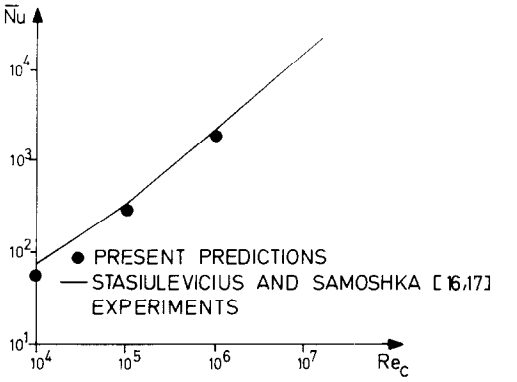

FIG. 12. Average Nusselt number $\overline{Nu}$ for fully-developed transverse flow through an in-line arrangement of $S_T \times S_L = 2 \times 2$ for $Pr = 0.7$.

The predicted effect of Prandtl number on the overall heat transfer is shown in Fig. 13, where $\overline{Nu}$ is given as a function of Re_c for a staggered arrangement of $S_T \times S_L = 1.3 \times 1.0$ for various Prandtl numbers. Very good agreement is observed with the measurements of Stasiulevicius and Samoshka [16, 17] for $Pr = 0.7$, which are also present in the figure. It can also be seen that $\overline{Nu}$ uniformly increases with Pr, thus suggesting that its effect can be easily correlated by using as ordinate the product $\overline{Nu}\ Pr^c$, where c is a constant. Figure 14 shows such a correlation, where $c = -0.36$.

3.4. *Heat transfer under conditions of uniformly inclined fully-developed flow*

3.4.1. *Equations and boundary conditions.* In this case it is assumed that the bulk velocity vector makes the

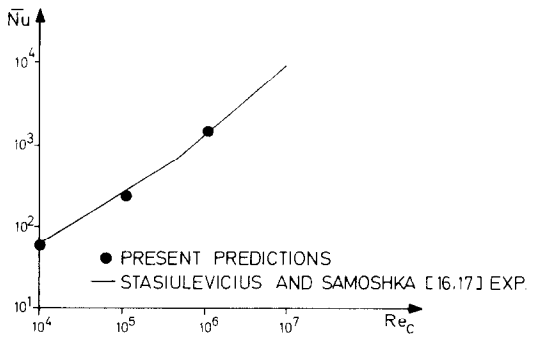

FIG. 11. Average Nusselt number $\overline{Nu}$ for fully-developed transverse flow through an in-line arrangement of $S_T \times S_L = 1.3 \times 1.3$ for $Pr = 0.7$.

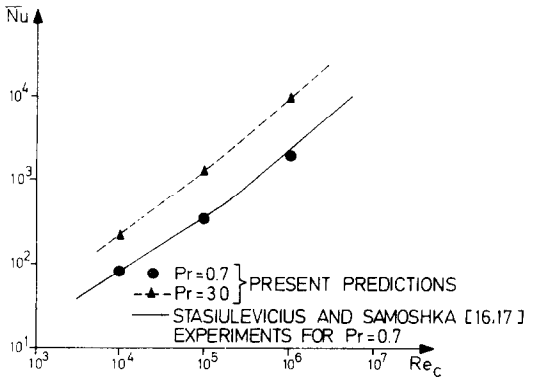

FIG. 13. Average Nusselt number $\overline{Nu}$ for fully-developed transverse flow through staggered arrangement of $S_T \times S_L = 1.3 \times 1$ for $Pr = 0.7$ and 30.

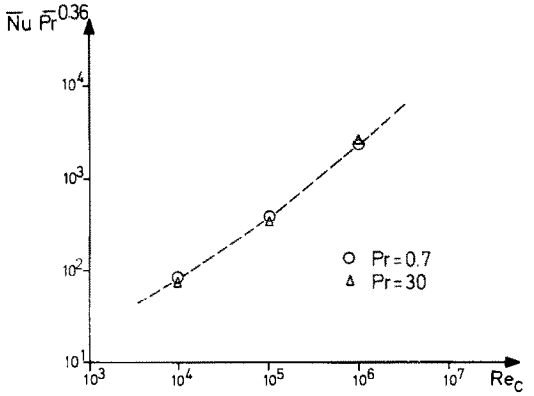

FIG. 14. Heat transfer correlation ($\overline{Nu}\,Pr^{-0.36}$ vs Re_c) for fully-developed transverse flow through a staggered arrangement of $S_T \times S_L = 1.3 \times 1$.

same angle with the tubes everywhere. The condition of full development of flow and heat transfer implies that all derivatives in the governing equations (1) and (2) with respect to the axial direction ζ vanish, with the exception of terms $\partial p/\partial\zeta$ and $\partial(\rho wT)/\partial\zeta$, which are non-zero. The transport equations take, therefore, the form of equation (12) (for $\Phi = u, v, w, k, \varepsilon$) and the continuity relationship takes the form of equation (14). The energy equation becomes

$$\frac{1}{l_\xi l_\eta}\frac{\partial}{\partial\xi}(\rho l_\eta uT) + \frac{1}{l_\xi l_\eta}\frac{\partial}{\partial\eta}(\rho l_\xi vT) + \frac{\partial}{\partial\zeta}(\rho wT) - \frac{1}{l_\xi l_\eta}\frac{\partial}{\partial\xi}\left(\Gamma_{T,\mathrm{eff}}\frac{l_\eta}{l_\xi}\frac{\partial T}{\partial\xi}\right) - \frac{1}{l_\xi l_\eta}\frac{\partial}{\partial\eta}\left(\Gamma_{T,\mathrm{eff}}\frac{l_\xi}{l_\eta}\frac{\partial T}{\partial\eta}\right) = 0. \quad (16)$$

Because of the simplification performed, the solution can be confined to a single cross-sectional plane ξ–η with the terms $\partial p/\partial\zeta$ and $\partial(\rho wT)/\partial\zeta$, associated with the axial coordinate ζ, treated as follows: the pressure gradient term $\partial p/\partial\zeta$ (contained in the source term of the w-momentum equation) is prescribed as an input or it is adjusted during the solution procedure so that the desired axial mass flow rate is obtained, as was the case with purely axial flow. The axial temperature gradient term $\partial(\rho wT)/\partial\zeta$, for the case of uniform wall heat flux boundary condition, can be easily calculated [1] as:

$$\frac{\partial(\rho wT)}{\partial\zeta} = \rho w\left(\frac{\dot{Q}\cos\Theta}{\dot{m}_c c_p P_L \sin\Theta + \dot{m}_a c_p P_A \cos\Theta}\right) \quad (17)$$

where P_L is the longitudinal pitch of the bank (Fig. 2) and P_A is the dimension of the solution domain in the axial direction (Fig. 3). It is then inserted as a source term in the energy equation (16), as was the case with the purely axial flow of Section 3.2.1.

The condition of full development in the transverse direction is employed for the imposition of boundary conditions at boundaries BA and GD of the solution domain (Fig. 9) in the same way as in the case of purely transverse fully-developed flow (Section 3.3.1), with the exception that the increase in bulk fluid temperature DT_b is not, in the present instance, calculated by equation (15) but by

$$DT_b = (T_b)_{DG} - (T_b)_{BA}. \quad (18)$$

In the above relation $(T_b)_{DG}$ is the bulk temperature through line DG given by

$$(T_b)_{DG} = \frac{\int_{DG}\rho u c_p T\,d\eta}{\int_{DG}\rho u c_p\,d\eta} \quad (19)$$

and $(T_b)_{BA}$ is the bulk temperature through line BA, given by a relation similar to (19).

The boundary condition of uniform wall heat flux is imposed on the solid boundaries (i.e. tube walls AJI and HGF, Fig. 9) of the solution domain while on the boundaries BCDE and IH (Fig. 9), which are planes of symmetry, v-velocity is zero as are the normal gradients of temperature and of all other variables.

3.4.2. *Results.* The predicted average Nusselt number $\overline{Nu}^h$ (based on the hydraulic diameter) as a function of the axial Reynolds number Re_a^h for various values of the transverse Reynolds number Re_c is shown in Fig. 15. These results relate to a staggered arrangement of $S_T \times S_L \doteq 2.42 \times 1.64$ for $Pr = 50$ and the inclination angles Θ are marked at various locations along the curves.

For constant, non-zero Re_c the pattern of the curves is as follows:

(a) For the higher values of Θ, $\overline{Nu}^h$ is practically constant and equal to the corresponding value for purely transverse flow, since the influence of the axial flow component is negligibly small.

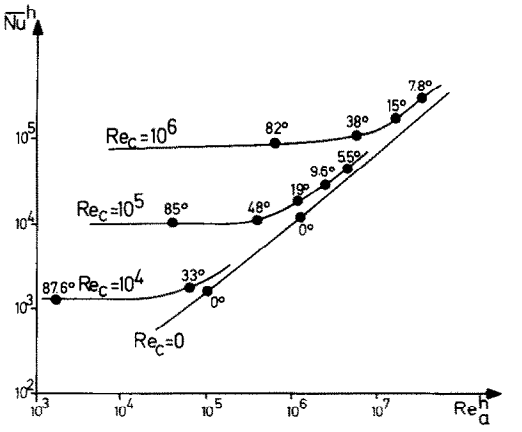

FIG. 15. Predicted average Nusselt number $\overline{Nu}^h$ as a function of the axial Reynolds number Re_a^h with the transverse Reynolds number Re_c as a parameter, for fully-developed inclined flow ($Pr = 50$) through a staggered arrangement of $S_T \times S_L = 2.42 \times 1.64$. Inclination angles Θ are marked along the curves.

(b) For the intermediate values of Θ, $\overline{Nu}^h$ increases with Re_a^h as does the slope of the $\overline{Nu}^h$ vs Re_a^h curve, due to the increasing effect of the axial flow component, which causes the boundary layer on the tube surfaces to be thinner, thus increasing the heat transfer coefficient.

(c) For the lower values of Θ, the $\overline{Nu}^h$ vs Re_a^h lines tend asymptotically to the line for $Re_c = 0$ (i.e. purely axial flow, $\Theta = 0°$).

Similar predictions to the above are shown in Fig. 16, which relates to a closely-spaced in-line arrangement of $S_T \times S_L = 1.3 \times 1.3$ for $Pr = 10$. In this figure, the line corresponding to $Re_c = 0$ (i.e. purely axial flow, $\Theta = 0°$) represents an empirical correlation for circular ducts taken from [14] but the error in using such correlations is not more than 12% according to Fig. 6 (Section 3.2.2.).

The conclusions drawn from Figs. 15 and 16 discussed above may be summarized as follows:

(i) Inclined flows exhibit higher heat transfer rates than purely axial ones.

(ii) For the same Re_c, inclined flows exhibit higher heat transfer rates than purely transverse ones. Thus at a fixed Re_c, $\overline{Nu}^h$ increases with decreasing inclination angle Θ or increasing Re_a^h.

(iii) At a fixed Re_a^h, $\overline{Nu}^h$ increases with Θ or Re_c.

It is noteworthy that the effect of the transverse flow component in highly-axial flows (e.g. $\Theta < 5°$) is less strong in a turbulent than in a laminar inclined flow [1] because in the former case the resistance to heat transfer (for intermediate and high Prandtl numbers, i.e. $Pr > 0.5$) is confined to the region near the wall surfaces so that the distortion of the axial velocity distribution (caused by the transverse flow component) within the cross-section plays a less important role in the overall heat transfer performance.

Predictions similar to those of Fig. 15 but for a fluid of a different Prandtl number ($Pr = 100$) are shown in Fig. 17. Comparison of these figures reveals that $\overline{Nu}^h$ increases with Pr in a practically uniform way thus suggesting that the effect of the latter can be eliminated by replotting as $\overline{Nu}^h Pr^{-0.36}$ vs Re_a^h, as shown in Fig. 18.

The influence of the inclination on the overall heat transfer performance is shown in a more compact form in Fig. 19(a), which relates to a staggered arrangement of $S_T \times S_L = 2.42 \times 1.64$ for a fluid of $Pr = 50$. Here the $\overline{Nu}^h$ predictions of Fig. 15 are replotted (using interpolation where necessary) as a function of the Reynolds number of the inclined flow Re^h (based on the hydraulic diameter) for fixed angles of inclination Θ. It is evident from this figure that for a constant value of Θ, $\overline{Nu}^h$ increases with Re^h as is the case with purely axial or transverse flow. At a fixed value of Re^h, $\overline{Nu}^h$ increases

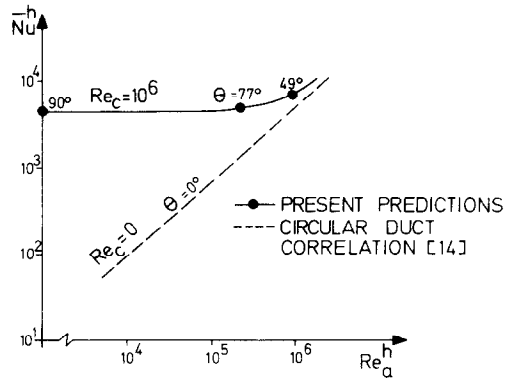

FIG. 16. Predicted average Nusselt number $\overline{Nu}^h$ as a function of the axial Reynolds number Re_a^h at transverse Reynolds numbers $Re_c = 10^6$ and 0, for fully-developed inclined flow ($Pr = 10$) through an in-line arrangement of $S_T \times S_L = 1.3 \times 1.3$. Inclination angles Θ are marked along the curves.

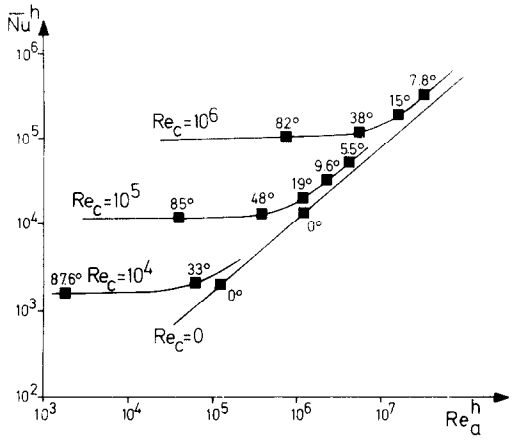

FIG. 17. Predicted average Nusselt number $\overline{Nu}^h$ as a function of the axial Reynolds number Re_a^h with the transverse Reynolds number Re_c as a parameter, for fully-developed inclined flow ($Pr = 100$) through a staggered arrangement of $S_T \times S_L = 2.42 \times 1.64$. Inclination angles Θ are marked along the curves.

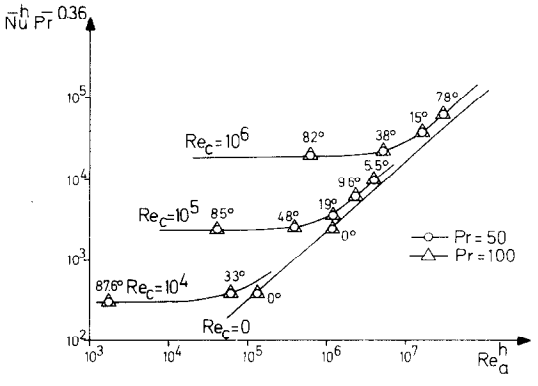

FIG. 18. Predicted $\overline{Nu}^h Pr^{-0.36}$ as a function of the axial Reynolds number Re_a^h with the transverse Reynolds number Re_c as a parameter for fully-developed inclined flow through a staggered arrangement of $S_T \times S_L = 2.42 \times 1.64$. Inclination angles Θ are marked along the curves.

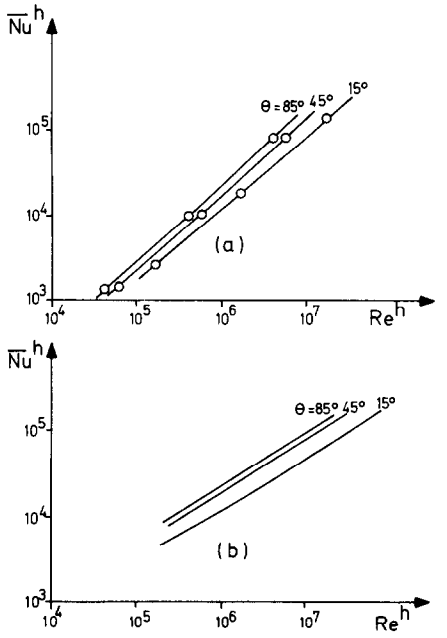

FIG. 19. Predicted average Nusselt number $\overline{Nu}^h$ for fully-developed inclined flow through a staggered arrangement of $S_T \times S_L = 2.42 \times 1.64$, as a function of the Reynolds number Re^h of the inclined flow for constant values of the inclination angle Θ ($Pr = 50$): (a) present predictions and (b) Dwyer [18] correlation.

with Θ, the maximum being obtained for purely transverse flow, as expected. The increase of $\overline{Nu}^h$ with Θ at a constant Re^h is, however, not uniform: a rapid increase is observed for Θ less than about 45°, while for the higher values of Θ the rate of increase falls. These trends are in qualitative agreement with those predicted by the Dwyer [18] correlation, as can be seen by comparing Figs. 19 (a) and (b); there is, however, a disagreement in the slope of the two sets of curves. The above-mentioned correlation is

$$\overline{Nu}^h = f\left(\frac{\sin\Theta + \sin^2\Theta}{1+\sin^2\Theta}\right)^{1/2}(4.6 + 0.193\, Pe^{0.614}) \quad (20)$$

where f is an empirical coefficient, which is stated to be a function of the geometrical characteristics of the tube arrangement considered and Pe is the Péclet number. For the purpose of the present comparison, f has been fixed by tuning the correlation to fit the present predictions at $Re^h = 10^6$ and $\Theta = 85°$. It has to be noted that the Dwyer [18] correlation (20) does not hold in the limiting case of purely axial flow, i.e. it gives $\overline{Nu}^h = 0$ for $\Theta = 0°$.

4. CONCLUSIONS

In the limiting case of heat transfer under conditions of purely axial fully-developed flow, the prediction procedure developed has been found to work satisfactorily within the limitations imposed by the neglect of turbulence-driven secondary motions and the general drawbacks of the k–ε model at Reynolds numbers in the transition region and just above.

In the limiting case of heat transfer under conditions of purely transverse fully-developed flow, the present procedure worked successfully for high Reynolds numbers. Transition and low Reynolds number effects could not be predicted due to deficiencies of the turbulence model employed to simulate these effects.

The present prediction procedure has also been found to work satisfactorily in the case of heat transfer under conditions of fully-developed inclined flow, although some uncertainties still exist due to lack of experimental data for comparison with the present predictions, which are the first of their kind. The main conclusions drawn are:

(a) At a fixed value of transverse Reynolds number Re_c, the predicted average Nusselt number $\overline{Nu}^h$ is independent of the axial Reynolds number Re_a^h for the higher values of inclination angle Θ, it increases with Re_a^h for the intermediate Θ and for the lower values of Θ the $\overline{Nu}^h$ vs Re_a^h curve tends asymptotically to the curve for purely axial flow, which lies below. This behaviour suggests that: inclined flows exhibit higher heat-transfer rates than purely axial ones; at fixed Re_c inclined flows exhibit higher heat transfer rates than purely transverse ones; and at fixed Re_a^h, $\overline{Nu}^h$ increases with Θ or Re_c.

(b) At a fixed Reynolds number Re^h of the inclined flow, $\overline{Nu}^h$ increases with Θ, the maximum value being obtained for purely transverse flow and the minimum for purely axial flow. At a fixed Θ, $\overline{Nu}^h$ increases with Re.

REFERENCES

1. K. A. Antonopoulos, Prediction of flow and heat transfer in rod bundles. Ph.D. thesis, Imperial College of Science and Technology, London (1979).
2. K. A. Antonopoulos, The simulation of turbulent tube bank flow, Proc. of the International '84 Athens Conference for Modelling and Simulation, AMSE, France (1984).
3. E. M. Sparrow, A. L. Loeffler and H. A. Hubbard, Heat transfer to longitudinal laminar flow between cylinders, *Trans. Am. Soc. mech. Engrs. J. Heat Transfer* **83**, 415–422 (1961).
4. O. E. Dwyer and H. C. Berry, Heat transfer to liquid metals flowing turbulently and longitudinally through closely spaced rod bundles, part I, *Nucl. Engng Des.* **23**, 273–294 (1972).
5. J. Pfann, Turbulent heat transfer to longitudinal flow through a triangular array of circular rods, *Nucl. Engng Des.* **34**, 203–219 (1975).
6. R. G. Deissler and M. F. Taylor, Analysis of axial turbulent flow and heat transfer through banks of rods or tubes, TID-7529, *Reactor Heat-Transfer Conference*, New York, Vol. 1, pp. 416–461 (1957).
7. R. F. Le Feuvre, Laminar and turbulent forced convection precesses through in-line tube banks. Ph.D. thesis, Imperial College of Science and Technology, London (1973).
8. T. H. Massey, The prediction of flow and heat-transfer in banks of tubes in cross-flow. Ph.D. thesis, Central

Electricity Research Laboratories, Leatherhead, Surrey (1976).
9. B. E. Launder and D. B. Spalding, *Mathematical Models of Turbulence*. Academic Press, London (1972).
10. J. Bloom, Experimental determination of the turbulent Prandtl number in a developing temperature boundary layer, Heat Transfer Conference, paper FC 2.2, Paris (1970).
11. D. B. Spalding, Contribution to the theory of heat transfer across a turbulent boundary layer, *Int. J. Heat and Mass Transfer* **7**, 743–761 (1964).
12. C. L. V. Jayatillaka, The influence of Prandtl number and surface roughness on the resistance of the laminar sublayer to momentum and heat transfer. Ph.D. thesis, University of London (1967).
13. L. S. Caretto, A. D. Gosman, S. V. Patankar and D. B. Spalding, Two calculation procedures for steady, three-dimensional flows with recirculation, *Proc. Third Int. Conference on Numerical Methods in Fluid Mechanics*, Vol. 2, pp. 60–68. Springer Verlag (1972).
14. W. M. Kays, *Convective Heat and Mass Transfer*. Tata McGraw-Hill, New Delhi (1975).
15. G. A. Mikhaylov, *Sovietskoye Kotloturbostroyeniye*, No. 12, p. 434 (1939).
16. J. K. Stasiulevicius and P. S. Samoshka, *Liet. TSR Mokslų Akad. Darb.* ser. B 4(35), p. 77 and p. 83 (1963).
17. J. K. Stasiulevicius and P. S. Samoshka, *Liet. TSR Mokslų Akad. Darb.* ser. B 4(55), p. 133 (1968).
18. O. E. Dwyer, Liquid metal heat-transfer, BNL 11936R (1969).

TRANSFERT THERMIQUE DANS UNE GRAPPE DE TUBES SOUS DES CONDITIONS D'ECOULEMENT TURBULENT ET INCLINE

Résumé—Il s'agit d'estimer le transfert thermique dans des arrangements de tubes, dans des conditions d'écoulement turbulent établi, incliné par rapport à l'axe des tubes, en incluant les cas limites de l'écoulement purement axial et transversal. Les équations qui gouvernent l'écoulement et le transfert thermique sont exprimés en coordonnées curvilinéaires et résolues par la méthode des différences finies. Les effets de la turbulence sont simulés par le 'modèle k–ε de turbulence'. Des résultats sont comparés avec des données expérimentales et théoriques dans les cas de l'écoulement purement axial et purement transverse. Une information nouvelle est fournie quant à l'influence de l'inclinaison de l'écoulement sur le transfert thermique.

WÄRMEÜBERGANG AN ROHRBÜNDELN BEI TURBULENTER, ZUR ACHSE DER ROHRE GENEIGTER STRÖMUNG

Zusammenfassung—Die vorliegende Arbeit behandelt die Berechnung des Wärmeübergangs an Rohrbündeln bei voll ausgebildeter, turbulenter Strömung, die zur Achse der Rohre geneigt ist, einschließlich der Grenzfälle reiner Axial- und reiner Querströmung. Die Differentialgleichungen für Strömung und Wärmeübertragung sind in gekrümmten Koordinaten formuliert und werden mit der Finite-Differenzen-Methode gelöst. Die Einflüsse der Turbulenz werden mit dem k–ε-Turbulenz-Modell berücksichtigt. Die Ergebnisse werden mit theoretischen und experimentellen Daten für die reine Axial- und die reine Querströmung verglichen. Es ergeben sich neue Erkenntnisse über den Wärmeübergang für eine gegen die Achse geneigte Strömung.

ТЕПЛООБМЕН В ПУЧКЕ ТРУБ В УСЛОВИЯХ ТУРБУЛЕНТНОГО ТЕЧЕНИЯ ПОД РАЗНЫМИ УГЛАМИ К ТРУБАМ

Аннотация—В настоящей работе дан расчет теплообмена в пучках труб в условиях турбулентного полностью развитого течения, поразному ориентированного по отношению к осям труб, включая предельные случаи чисто продольного и чисто поперечного обтекания. Дифференциальные уравнения, определяющие течение и теплоперенос, представлены в криволинейных координатах и решены конечно-разностным методом. Турбулентность рассчитана при помощи 'k–ε'-модели. Результаты сравниваются с теоретическими и экспериментальными данными в случаях чисто продольного и чисто поперечного обтекания. Получены новые данные по влиянию наклона течения на теплообмен.